Control of a Four-Leg Converter for the Operation of a DFIG Feeding Stand-Alone Unbalanced Loads

Gonzalo Carrasco, César A. Silva, *Member, IEEE*, Rubén Peña, *Member, IEEE*, and Roberto Cárdenas, *Senior Member, IEEE*

***Abstract*—This paper presents a topology for a three--phase generation system for an isolated unbalanced load fed by a doubly fed induction generator with a neutral wire to include single-phase loads. The challenges of unbalanced loads connected to the system are presented along with a proposal for mitigating current imbalance by employing a four-leg rectifier. The proposed compensation method is based on the sequence decomposition analysis, and thus, it is based on previous works that use current control in double synchronous reference frames. Nevertheless, a conceptual analysis is presented that vindicates the use of resonant controllers in the stationary abc frame.**

***Index Terms*—Converters, electric current control, micorgrids, static VAR compensators, wind energy generation.**

I. Introduction

In a stand-alone wind energy conversion system, a doubly fed induction generator (DFIG) may directly feed into a load, such as a small village. For these applications, the unbalanced nature of the loads could be a problem for the DFIG, mainly because both the load power and the torque at the machine shaft would be pulsating. This will also result in a current derating of the machine to prevent localized winding heating [1]–[3]. Several works have been presented in the last decade aiming to mitigate unbalanced currents [2], [4]–[7]. Most of these works apply to grid-connected DFIGs, where there is a demand for fault ride through in the case of unbalanced voltages sags. The problem is different in stand-alone systems since the generator imposes the voltage, but the loads demand unbalanced currents. Negative-sequence currents can be compensated by the shunt-connected grid-side converter (GSC), as proposed in [8]–[10]. In these works, only three-phase links without a neutral connection are studied. For systems including single-phase loads, a neutral wire must be provided for a phase-to-neutral load connection; thus, the zero-sequence current of the load needs a low-impedance path to maintain the voltage balance. This is presented in [11], where single-phase loads are wired to the start-connected stator of a DFIG, resulting in common mode current flowing through the stator.

This work is partially based on the preliminary work presented in [11], where negative-sequence currents are regulated in the negative synchronous reference frame (SRF) to supply the load demands, and the positive-sequence current is used to regulate the dc-link voltage, and it is controlled in the positive SRF. If a neutral wire is included, complete balance is not achieved with this method due to common mode current. Thus, localized heating may still be produced in the DFIG, and therefore, one phase may limit the total current capability of the system. Until recently, four-wire unbalanced stand-alone systems fed by the DFIG have not received much attention. One exception is the work in [12], where the use of a four-leg GSC is proposed to provide a path for the load neutral current to avoid voltage distortion at the load. Nevertheless, in [12], the full advantage of this new degree of freedom is not exploited, since the modulated voltage of the fourth leg is kept constant at half the dc-link voltage. In the present work, a neutral connection to the machine is provided in order to naturally achieve sinusoidal balanced voltages at the load, and the four-leg inverter is used to balance the stator current of the generator by means of the active modulation of the fourth leg in order to improve the dc-link utilization.

Four-leg-converter modulation has been presented from the space vector modulation and the carrier-based pulsewidth modulation point of view [13]–[16]. Finally, several methods for sequence decomposition have been proposed using a phase-locked loop (PLL) for grid synchronization under faulty conditions [17]–[20]. Furthermore, sequence decomposition is also necessary for current feedback when the control is done in a double synchronous reference frame (DSRF) [8]–[11]. In this paper, the authors postulate that the dynamic performance of the current controllers is better if such sequence separation algorithms are avoided in the feedback path. This leads to the use of only resonant controllers at the natural abc coordinates to naturally achieve positive-, negative-, and zero-sequence control without sequence separation algorithms.

II. Standalone DFIG With Neutral Connection

Single-phase loads require a neutral connection, i.e., a four-wire system. On the other hand, zero-sequence currents are not torque producing in a start-connected machine, but the presence of an imbalance will limit the operation of the machine to the condition where the largest magnitude of the phase currents

Manuscript received May 7, 2014; revised July 17, 2014 and August 18, 2014; accepted September 16, 2014. Date of publication October 21, 2014; date of current version May 15, 2015. This work was supported in part by the MECESUP under Grant FSM0601, in part by the Centro Científico-Tecnológico de Valparaíso (CCTVal) under Grant FB0821, and in part by the Fondecyt 1120683 Project.

G. Carrasco and C. A. Silva are with the Electronics Engineering Department, Universidad Técnica Federico Santa María, 110-V Valparaíso, Chile (e-mail: gonzalo.carrasco@postgrado.usm.cl; cesar.silva@usm.cl).

R. Peña is with the Electrical Engineering Department, University of Concepción, 160-C Concepción, Chile (e-mail: rupena@udec.cl).

R. Cárdenas is with the Electrical Engineering Department, University of Chile, 1058 Santiago, Chile (e-mail: rcd@ieee.org).

Color versions of one or more of the figures in this paper are available online at http://ieeexplore.ieee.org.

Digital Object Identifier 10.1109/TIE.2014.2364155

0278-0046 © 2014 IEEE. Personal use is permitted, but republication/redistribution requires IEEE permission.
See http://www.ieee.org/publications_standards/publications/rights/index.html for more information.

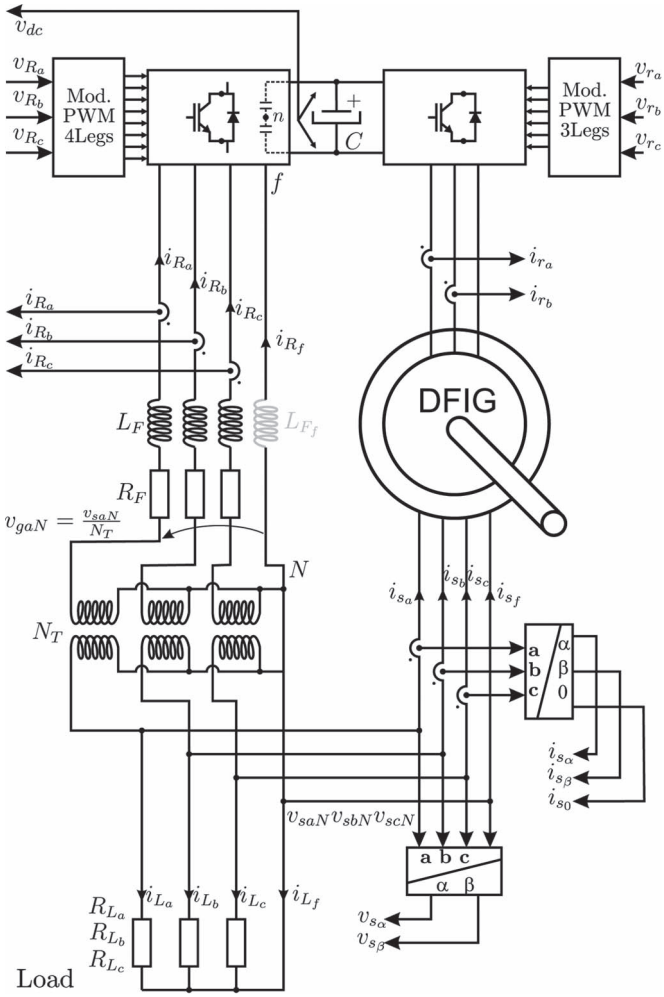

Fig. 1. Electric scheme of the generation system.

reaches the per-phase rating of the machine. This consideration highlights the need for compensation of the whole imbalance, including for zero-sequence current.

Recently, the need for zero-sequence compensation in a DFIG has been addressed in [12], balancing the load voltages by means of a four-leg GSC without neutral connection to the machine. In this paper, it is considered better to have a neutral connection between the machine and the load to naturally balance the load voltage, even if the full capacity of the GSC is reached. Therefore, the four-leg GSC acts as a shunt current imbalance compensator, even for the zero sequence. The power stage of the system is shown in Fig. 1, where the load, DFIG, and GSC interconnection are shown. The variables used are defined as follows:

i_{rd}	rotor current to be controlled;
v_{rd}	rotor voltage, actuation variable;
$-(L_m/L_s)v_{sd}$	input disturbance to the plant in d;
$(L_m/L_s\tau_s)\psi_{sd}$	input disturbance to the plant in d;
$\omega_{sl}\ \sigma\ L_r\ i_{rq}$	input disturbance to the plant in d;
i_{rq}	rotor current to be controlled;
v_{rq}	rotor voltage, actuation variable;
$\omega_r(L_m/L_s)\psi_{sd}$	input disturbance to the plant in q;
$-(L_m/L_s)v_{sq}$	input disturbance to the plant in q;
$-\omega_{sl}\ \sigma\ L_r\ i_{rd}$	input disturbance to the plant in q;

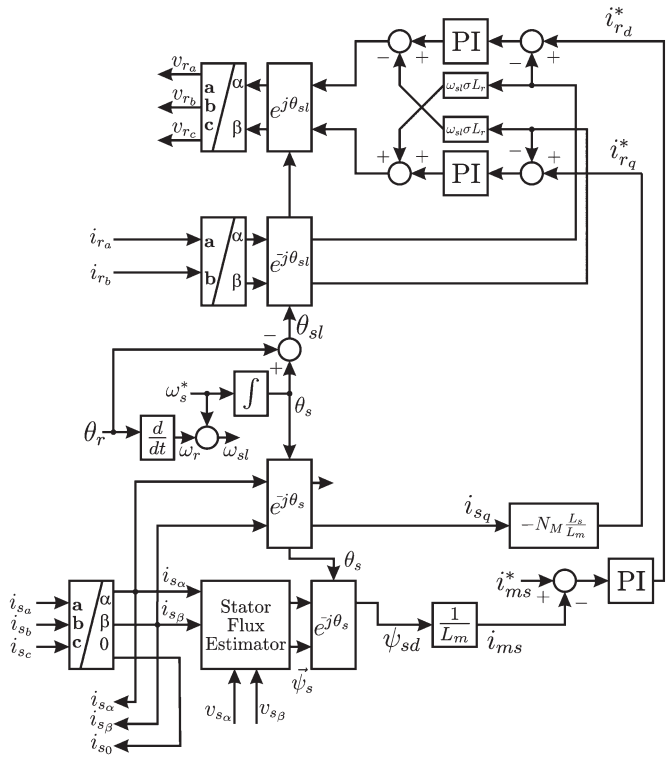

Fig. 2. Control scheme for the DFIG magnetizing current.

ω_m	mechanical speed of the shaft;
ω_r	electrical rotor speed ($\omega_r = \omega_m p$);
p	number of pole pairs;
L_m	magnetizing inductance;
$L_{\sigma s}$	leakage stator inductance;
$L_{\sigma r}$	leakage rotor inductance;
L_s	stator inductance ($L_s = L_{\sigma s} + L_m$);
L_r	rotor inductance ($L_r = L_{\sigma r} + L_m$);
σ	total leakage factor ($\sigma = 1 - L_m^2/(L_s L_r)$).

Finally, to achieve maximum utilization of the dc-link voltage of the GSC, a controlled zero-sequence voltage, as proposed in [15], is actively modulated in the fourth leg of the GSC. This maximizes the actuation capability on the zero-sequence axis, as discussed in [14].

A. Vector Control of DFIG in Standalone

The current control of the DFIG changes the electrical torque according to the shaft speed in order to balance the power demanded by the loads with the power taken from the mechanical system. Vector control is achieved by regulating the rotor currents in a synchronous rotating frame orientated with the stator flux, following the scheme presented in [21]. In stand-alone operations, stator voltage control is achieved by regulating the magnetizing (i_{rd}) component of the rotor current. When the magnetizing current is controlled, the stator voltage is sufficiently stable. Only stator resistance and stator leakage inductance affect the regulation. Fig. 2 shows the control diagram of the DFIG. For the indirect vector control of the DFIG, the machine model is presented in the states' variables, stator flux $\vec{\psi}_s$ and rotor current $\vec{i}_r$, and equations

are analyzed in the positive SRF. The orientation is with $\vec{\psi}_s$; therefore, $\psi_{sd} = |\vec{\psi}_s|$, and $\psi_{sq} = 0$. Thus,

$$\tau_s \frac{d\psi_{sd}}{dt} + \psi_{sd} = \tau_s v_{sd} + L_m i_{rd} \quad (1)$$

$$0 = \tau_s v_{sq} + L_m i_{rq} - \omega_s \tau_s \psi_{sd} \quad (2)$$

$$R_{\sigma r}\left(\tau_{\sigma r}\frac{di_{rd}}{dt} + i_{rd}\right) = v_{rd} - \frac{L_m}{L_s}v_{sd} + \frac{L_m}{L_s \tau_s}\psi_{sd} + \omega_{sl}\sigma L_r i_{rq} \quad (3)$$

$$R_{\sigma r}\left(\tau_{\sigma r}\frac{di_{rq}}{dt} + i_{rq}\right) = v_{rq} + \omega_r \frac{L_m}{L_s}\psi_{sd} - \frac{L_m}{L_s}v_{sq} - \omega_{sl}\sigma L_r i_{rd}. \quad (4)$$

Equations (3) and (4) are used for the rotor current control; the reference for i_{rq} is taken from the flux linkage relation in the q-axis ($\psi_{sq} = 0$). Equation (2) is used to control the magnetizing current defined as $\psi_{sd} = L_s i_{sd} + L_m i_{rd} = L_m i_m$, with i_{rd} as the actuation variable.

B. Stator Negative- and Zero-Sequence Current Compensation in DSRF

The negative-sequence current compensation described in this section is based on what has been previously presented in [11], and it is included here mainly for the sake of completeness. Here, the problem of torque pulsations in the machine is solved by regulating balanced currents in the stator and rotor windings. The compensation method consists of the control of the positive- and negative-sequence currents in a double SRF. Nevertheless, this solution is not enough to balance the stator currents in a four-wire connection; therefore, a fourth leg in the converter and a resonant controller at fundamental frequency must be added in the control scheme so as to allow regulation of the zero-sequence current.

Having balanced stator currents indicates that GSC must supply the negative and zero sequences' currents in the three-phase loads. Current references for the negative and zero sequences of the GSC need to be calculated from the load currents. This scheme requires an explicit sequence decomposition in the feedback path. Perfect sequence decomposition is not possible during transient behavior, and thus, it inevitably adds a dynamic characteristic to the measurements. The equivalence between proportional–integral (PI) controllers in SRF and the cross-coupled resonant controllers used to regulate one of the sequences in a stationary frame has been demonstrated in [22] and [23]. Furthermore, resonant controllers in the $\alpha\beta$ frame without cross-coupling produce a symmetric frequency response to positive and negative sequences and, thus, are almost ideal for this application.

Furthermore, strictly speaking, the controllers in different coordinates cannot be perfectly equivalent, since that would require a perfect sequence decomposition to be used in DSRF control. In a real implementation of DSRF control, there is a filtering effect in the current feedback path due to the current sequence decomposition stage. Therefore, the resonant version must be better than the DSRF due to the elimination of the sequence decomposition stage. In summary, the well-known advantages of DSRF control are natural frequency adaptation in variable frequency applications and independent dynamic behavior that can be set for each sequence. On the other hand, resonant controllers are simpler and more efficient in constant frequency applications, and they are also better suited for systems where the positive- and negative-sequence impedance values are the same.

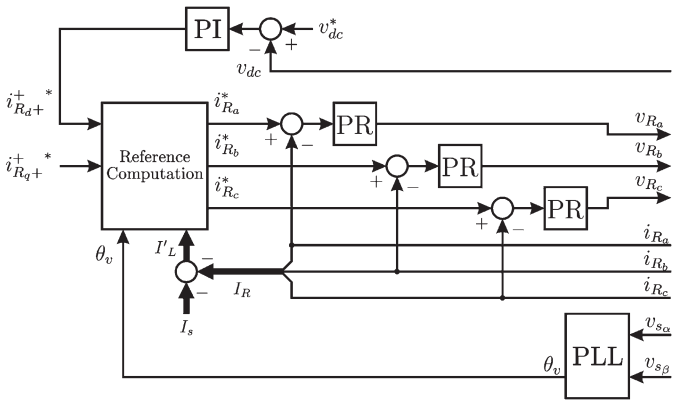

Fig. 3. Proposed control strategy using resonant or multiresonant controllers.

III. Neutral Current Compensation With Resonant Controllers in abc Coordinates

From the previous analysis, it follows that the current control of the GSC could be implemented in $\alpha\beta 0$ coordinates by means of resonant controllers. Here, it is argued that it is simpler to choose natural abc coordinates instead. In the power circuit shown in Fig. 1, inductances are added to the GSC as coupling filters. A neutral inductance is also shown (L_{Ff}), but it is not strictly necessary because the zero-sequence path has an equivalent inductance of $(L_a + L_b + L_c)/3$ from the abc filters. If $L_{Ff} = 0$, each phase is linearly independent of the others, i.e., the current in one phase does not produce disturbances in the other phases. In other words, they are naturally decoupled [see (5)–(7)]. Typically, abc to $\alpha\beta$ transformation is applied to three-wire systems where only two out of the three-phase currents are linearly independent, so the Clarke transformation orthogonalizes these two independent currents. This is not the case in the four-wire system where currents are naturally decoupled and, hence, are orthogonal.

The d and q components of positive- and negative-sequence currents and magnitude and relative phase shift of the zero-sequence current add up six degrees of freedom to be controlled. Thus, instead of controlling the six degrees of freedom of GSC currents separated in symmetrical components, these six degrees of freedom are controlled in the natural abc current frame, i.e., controlling the three magnitudes of a, b, and c fundamental GSC currents and their relative phase shift with respect to the stator voltage.

The proposed GSC current control is shown in Fig. 3. The advantage of using the same controllers in each phase is evident, since control tuning is performed for all phases at the same time. Therefore, the control scheme in Fig. 3 results in an easy implementation with control loops that are more intuitive and explicit.

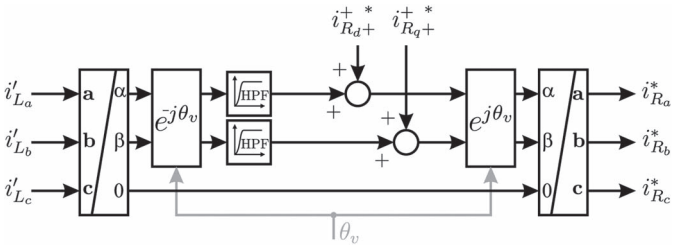

Fig. 4. One method to generate the current references for the resonant controllers.

Although this scheme does not need sequence separation for current feedback, this simple current control method still requires a relatively complex current reference computation algorithm. Indeed, current decomposition is necessary in order to find the current references, but it is achieved with low-order filters. Furthermore, this does not add dynamics to the current feedback. With the aim of balancing the currents in the DFIG stator, all of the negative and zero sequences, and ideally any distortion, should be supplied by the GSC. Additionally, the GSC should handle a fraction of the stator positive-sequence current (i.e., active power) to achieve regulation of the dc-link voltage [24]. The current references for the GSC are obtained with the scheme shown in Fig. 4, where the positive-sequence current of the load is filtered out. The positive-sequence current references $i^{+}_{R_{d_+}}$ and $i^{+}_{R_{q_+}}$ come, respectively, from the dc-link voltage controller and an arbitrary set point (usually zero).

With this scheme, it is possible to generate a proper reference in steady state for the fundamental and harmonic frequencies if the cutoff frequency of the high-pass filter is low enough. In fact, this scheme has the advantage of performing well for harmonic components, and thus, if the current controllers are able to follow their references perfectly, the GSC acts both as an active filter for harmonics and as a fundamental imbalance compensator.

For each phase, the model that relates the current of the GSC and its voltages, considering that the voltage at the secondary side of the transformer is $v_g = v_s/N_T$, is given by

$$v_{gaN} = R_{Fa} \cdot i_{Ra} + L_{Fa}\frac{di_{Ra}}{dt} + v_{Raf} - L_{F_f}\frac{di_{Rf}}{dt} \tag{5}$$

$$v_{gbN} = R_{Fb} \cdot i_{Rb} + L_{Fb}\frac{di_{Rb}}{dt} + v_{Rbf} - L_{F_f}\frac{di_{Rf}}{dt} \tag{6}$$

$$v_{gcN} = R_{Fc} \cdot i_{Rc} + L_{Fc}\frac{di_{Rc}}{dt} + v_{Rcf} - L_{F_f}\frac{di_{Rf}}{dt}. \tag{7}$$

Thus, with $L_{Ff} = 0$ and regarding v_g as an input disturbance, the per-phase transfer function of the plant to be controlled is

$$\frac{i_R(s)}{v_R(s)} = -\frac{1}{L_F s + R_F}. \tag{8}$$

The structure of a resonant controller can be easily understood by recalling the internal model principle for feedback control [25]. For the tracking of the fundamental reference, complex conjugate poles in the imaginary axis are needed at the same frequency of the reference, i.e., 50 Hz. Coupling between phases, if they exist, has the same frequency, and therefore, no

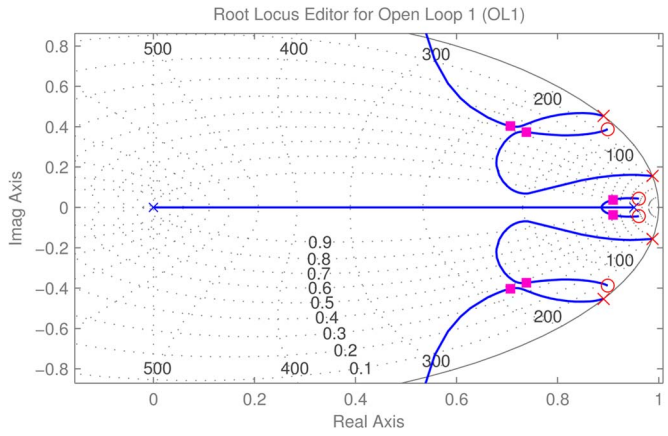

Fig. 5. Root locus of the closed-loop control.

extra poles in the controller are necessary. In continuous time, the transfer function of the resonator is

$$R(s) = \frac{2s}{s^2 + \omega_0^2}. \tag{9}$$

As presented in [23], this term can be understood as a frequency shift of the integrator in a PI controller on a positive SRF, and discarding the coupling term, resulting in the same response for the positive- and negative-sequence control. Therefore, the proportional-resonant controller is

$$C(s) = K_P + K_R\frac{2s}{s^2 + \omega_0^2} \tag{10}$$

which, in discrete time, has the following structure:

$$C(z) = \frac{KN0 + KN1z^{-1} + KN2z^{-2}}{1 - 2z^{-1}\cos(\omega_0 T_s) + z^{-2}} \tag{11}$$

where T_s is the sampling time for the current control. This controller gives three degrees of freedom: the real positioning of the conjugate complex zeros, the imaginary conjugate positioning of the complex zeros, and the proportional gain. In the case that more harmonics are to be tracked or rejected as disturbances, more resonances must be added, giving rise to a multiresonant structure. Results shown in the next sections are obtained using two resonances: at fundamental frequency and third harmonic due to the effect of the saturation of the machine, i.e.,

$$C(z) = \frac{KN0 + KN1z^{-1} + KN2z^{-2} + KN3z^{-3} + KN4z^{-4}}{(1 - 2z^{-1}\cos(\omega_0 T_s) + z^{-2})} \times \frac{1}{(1 - 2z^{-1}\cos(3\omega_0 T_s) + z^{-2})}. \tag{12}$$

The adjustment of the current regulator was done by means of zeros and gain manipulation in the root locus using MATLAB's SISO design tool (see Fig. 5). The design objective is to obtain a response as fast as possible while maintaining a relatively flat closed-loop Bode plot. The fast response is associated with the absolute decay in gain at the highest frequency possible. The flat response is desirable so as to prevent resonances that could amplify noise, disturbances, or transient

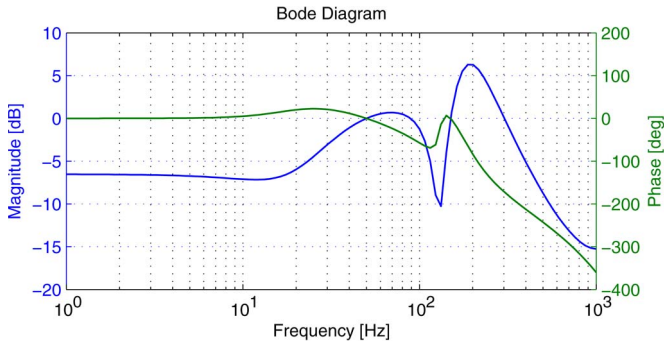

Fig. 6. Bode plot of the closed-loop control.

references. The Bode plot of the designed closed-loop response associated to the root locus in Fig. 5 is shown in Fig. 6.

Since the DFIG's fundamental voltage is expected to be balanced and can be estimated, PLL is not strictly necessary for the synchronization of the GSC; nevertheless, a PLL with negative-sequence cancelation was implemented in order to avoid potential phase distortion, which could be caused by heavily unbalanced loads.

IV. Simulation Results

The validation of the proposed control strategy is first done by means of simulations using the same parameters of the experimental setup. The most important parameters of the experimental setup are presented in Table I given in the Appendix. It is important to note that the current loop control has a sampling rate of $T_{s_i} = 0.5$ ms, and the voltage control loop works 20 times slower at $T_{s_v} = 10$ ms. The PI voltage regulator has a saturation of the current reference for the inner loops fixed to 14 A. All digital filters (including controllers) have the following structure:

$$H(z) = \frac{KN0 + KN1z^{-1} + \cdots + KNmz^{-m}}{1 - KD1z^{-1} - \cdots - KNnz^{-n}} \qquad (13)$$

where all the filter constants are listed in Table II in the Appendix.

Several tests were performed to observe how currents change under different conditions, always at subsynchronous speed, with the rotor frequency set at $\omega_r = 0.8(2\pi 50)$ rad/s. In the color version of this document, blue, green, red, and cyan represent phases a, b, c, and neutral, respectively, and d and q stator currents are depicted in blue and green, respectively.

With only the negative-sequence compensation implemented in the reference calculations, i_a is doubled with respect to the balance condition, and the results are shown in Fig. 7. To make the negative sequence of i_s evident if it exists, stator currents are shown in the positive SRF. Thus, in the steady-state condition, the positive sequence appears as dc signals, and the negative-sequence current would appear as a 100-Hz ripple, as can be seen from the first 0.05 s in Fig. 9 when the compensation is not activated. The fact that there is not such double-fundamental frequency when the negative-sequence compensation is activated in Figs. 7 and 8 shows good performance of the proposed scheme. When the negative sequence of i_s is regulated to zero,

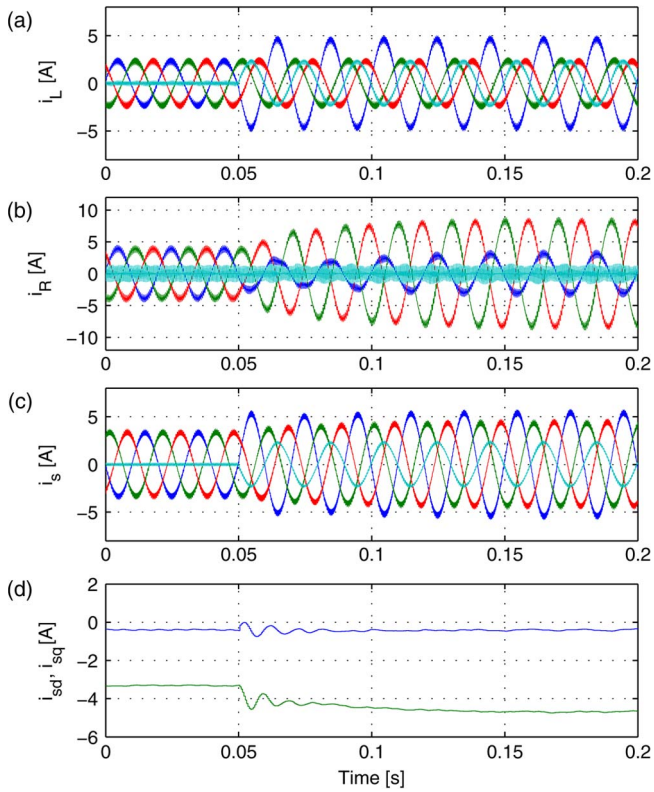

Fig. 7. Simulated load current imbalance with compensation of negative sequences. (a) Load currents. (b) GSC currents. (c) DFIG stator currents. (d) Positive SRF dq stator currents.

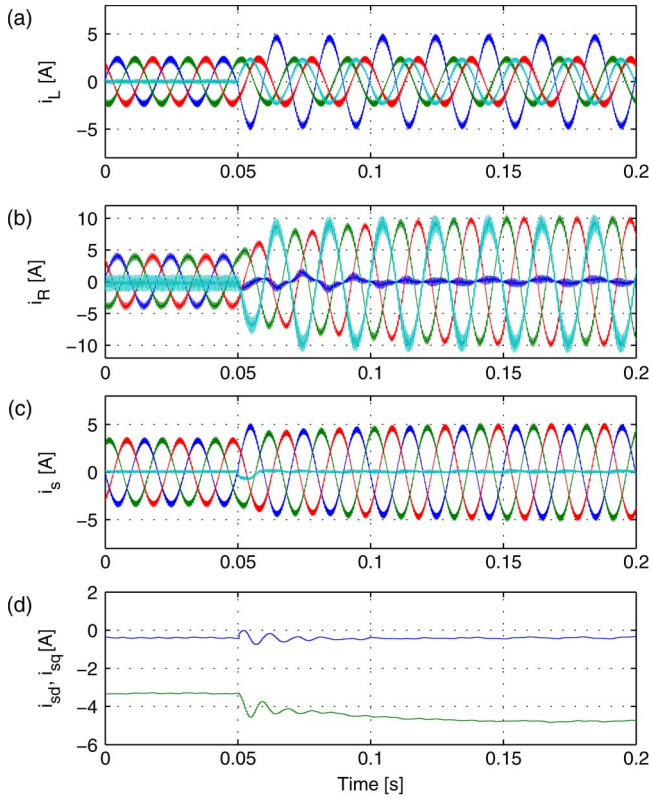

Fig. 8. Simulated load current imbalance with full compensation of imbalance. (a) Load currents. (b) GSC currents. (c) DFIG stator currents. (d) Positive SRF dq stator currents.

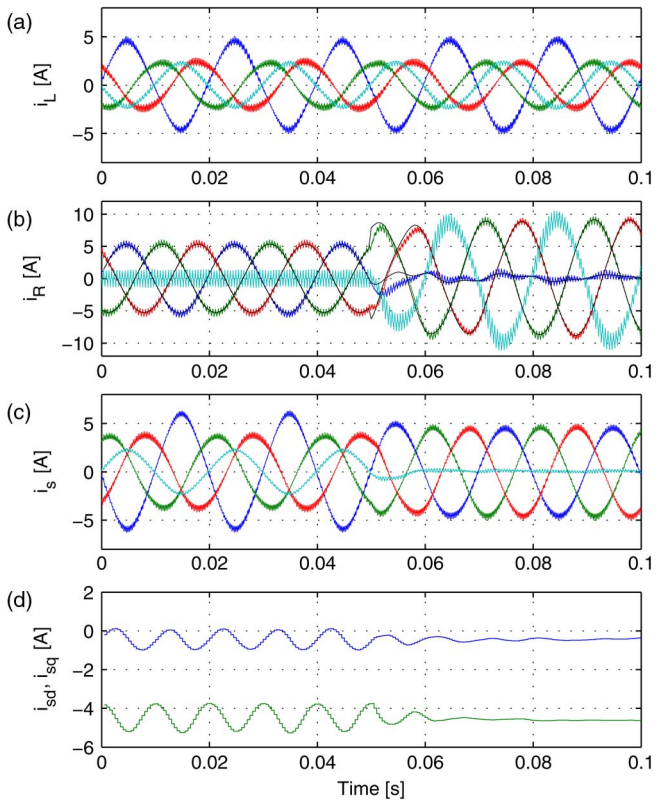

Fig. 9. Simulated turning negative and zero compensations on with unbalanced load. (a) Load currents. (b) GSC currents. (c) DFIG stator currents. (d) Positive SRF dq stator currents.

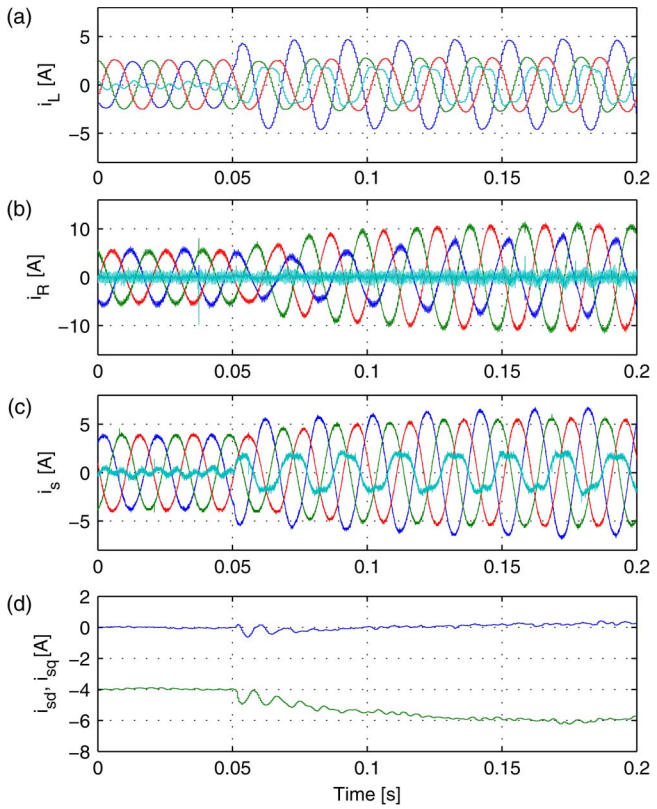

Fig. 10. Experimental load current imbalance with compensation of negative sequences. (a) Load currents. (b) GSC currents. (c) DFIG stator currents. (d) Positive SRF dq stator currents.

there is still an imbalance condition due to the zero-sequence current. Until now, the current in the fourth leg of the GSC has been regulated to zero, i.e., as if it was not connected. This corresponds to the best achievable result with a three-leg GSC (as proposed in [11]) when feeding systems with single-phase loads.

The GSC currents (i_R) show an increasing envelope after the imbalance due to the slow dynamic of the voltage regulation of the dc link, which is performed by the GSC. Consequently, there is more demand of power from the DFIG when doubling the a phase current; hence, at subsynchronous speed, there is an increase in active power demanded by the rotor to the RSC. This disturbs the dc-link voltage, and the GSC must demand more power from the stator (i.e., more positive-sequence currents). This outer control loop sets the reference $i^{+*}_{R_{d_+}}$ for the inner current loop as its actuation variable (see Fig. 4), and it is responsible for the slow envelope of the positive-sequence currents, taking several fundamental periods to reach steady state.

Fig. 8 shows the results of the load imbalance when the full compensation described in Fig. 4 is activated. In this case, the GSC provides the zero-sequence current that the load demands, and thus, the stator of the DFIG only delivers the positive-sequence currents demanded by the load and the GSC. In this result, it can be observed that the magnitude of the larger current (phase a) is reduced. The current capacity of the DFIG can be increased without causing local overheating by distributing the load evenly among phases. In Fig. 8(c), the fast regulation of the control system can be inferred: After the load imbalance, the stator currents are regulated to be balanced in about one fundamental period, i.e., negative and zero stator current sequences are regulated to zero.

The transient behavior of the resonant controllers is shown in Fig. 9 where the compensations are activated under a steady-state load imbalance. The GSC current references (black thin lines in the figure) are quickly followed to balance the stator currents in approximately one fundamental period. Thus, the reference tracking performed by the resonant controllers can be as fast as the PI controllers in DSRFs.

V. Experimental Results

The proposed control strategy is tested in a laboratory prototype, coded into an algorithm in C, and implemented in a dSPACE platform (ds1103). The circuit and control schemes in Figs. 1–3 make up the experimental setup. Fig. 1 shows a transformer (three-phase variable autotransformer) between the GSC and the stator of the DFIG, which is only necessary for the laboratory experimental setup due to the unsuitable turn ratio of the available DFIG. The low leakage inductance and negligible magnetizing current of the transformer prevent an undesirable effect on the system.

The control platform allows for the acquisition of data at the control sampling rate (T_{s_i}); thus, several graphics show variables taken at this rate. To observe the currents with the natural switching ripple of the two-level converters used as an inverter and four-leg GSC, measurements of the GSC currents,

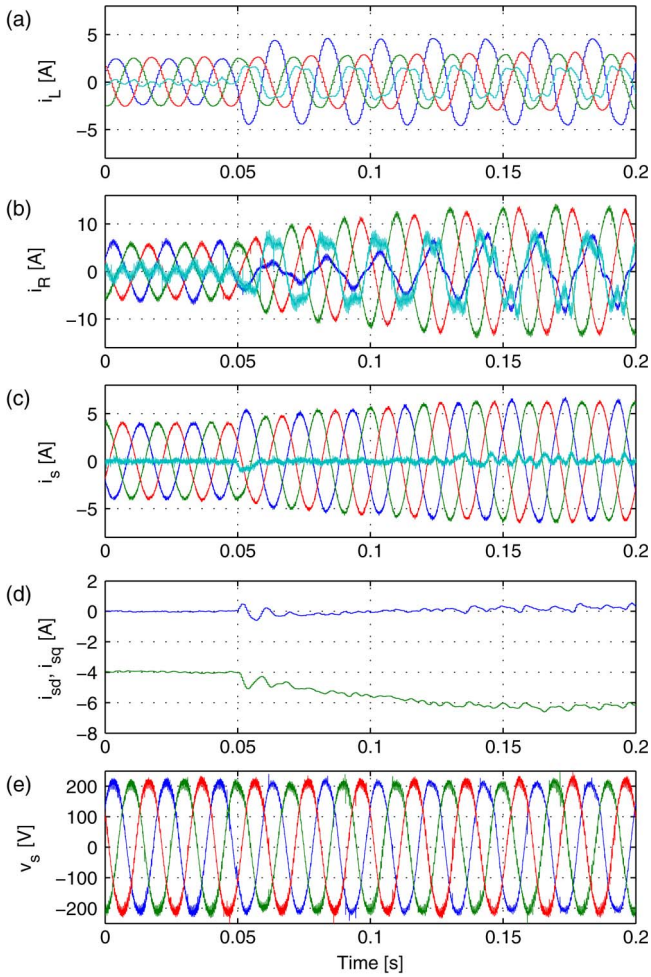

Fig. 11. Experimental load current imbalance with compensation of negative and zero sequences. (a) Load currents. (b) GSC currents. (c) DFIG stator currents. (d) Positive SRF dq stator currents. (e) Stator voltages.

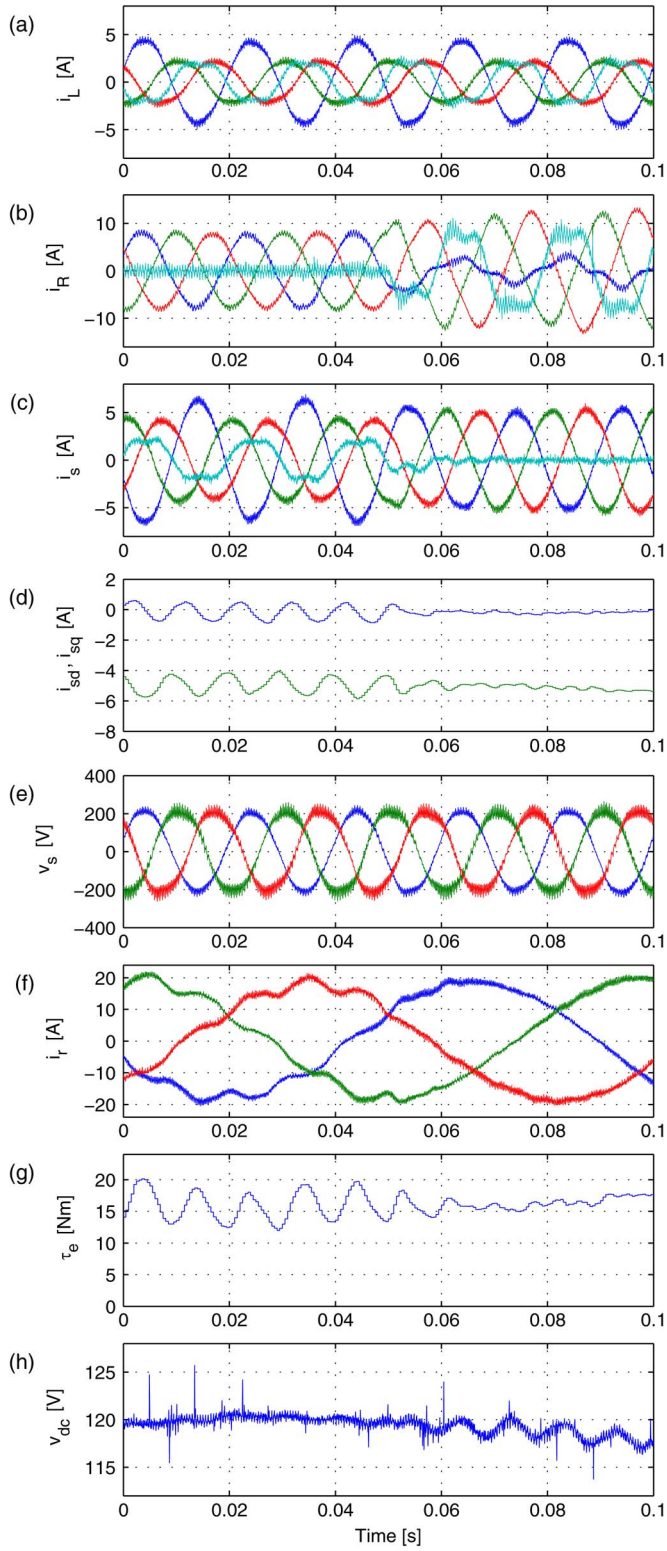

Fig. 12. Experimental turning negative and zero compensations on with unbalanced load currents. (a) Load currents. (b) GSC currents. (c) DFIG stator currents. (d) Positive flux SRF dq stator currents. (e) Stator voltages. (f) Rotor currents. (g) Torque. (h) DC-link voltage.

stator currents, and stator voltages were done with digital oscilloscopes (two Agilent DSO-X 3024A and a DSO-X 2024A). After capturing the data at the sampling rate of 40 kHz with the oscilloscopes, it was processed in MATLAB in order to be displayed. Modulation of the four-leg GSC was done as proposed in [15] at a carrier frequency of 2 kHz.

In Fig. 10, only the negative-sequence current compensation is enabled, and thus, the GSC is delivering the negative sequence demanded by the loads. The load currents (i_L) and, therefore, the stator currents of the DFIG have a third-harmonic component. This is due to the fact that the rotor current control regulates a sinusoidal magnetizing current, which produces a slightly distorted flux in the DFIG because the machine core operates near saturation. This distorted flux induces a distorted voltage at the stator terminals. Hence, resistive loads will demand a distorted current. The distortion in abc load currents (i_L) is not evident in Fig. 10, but as the third harmonic is common mode, it is visible in the neutral current, even at a balanced load condition.

The addition of a second resonance was implemented in order to compensate for the third-harmonic currents in addition to the fundamental. This means that a fourth-order multiresonant controller was adjusted for the plant (the constants are given in Table II in the Appendix). By using this multiresonant controller in each phase and with the reference calculation scheme in Fig. 4, it is possible to prevent the circulation of

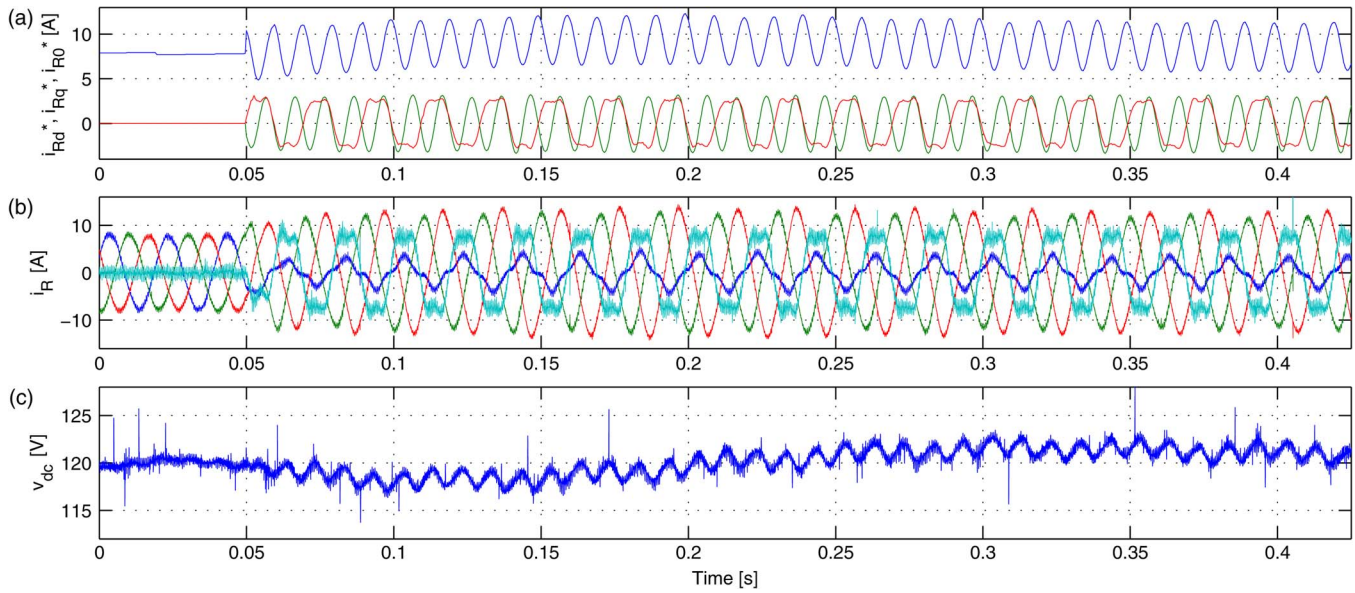

Fig. 13. Experimental turning negative and zero compensations on with unbalanced load currents (the same case of Fig. 12). (a) Reference current to the GSC in positive SRF after adding $i_{R_{d_+}}^+$ and $i_{R_{q_+}}^+$. (b) GSC currents. (c) DC-link voltage.

harmonic current in the stator. This is experimentally done to show that, with the right selection of the control structure, this control scheme behaves both as an imbalance compensator and as an active filter. In this case, it has a high gain at the two relevant frequencies.

The result in Fig. 10 has not yet taken full advantage of the capabilities of the fourth leg of the GSC since its current has been controlled to zero. The experimental result in Fig. 11 finally shows the effectiveness of the complete proposed control scheme, where full compensation of the stator current imbalance is obtained, and the negative and zero sequences of the load are now delivered by the GSC, thus including a strong third-harmonic distortion. It can be observed that the zero-sequence current regulation takes less than a fundamental period and that the negative-sequence stator current (as ripple of 100 Hz in $i_{s_d}^+$ and $i_{s_q}^+$) is regulated to zero in about one fundamental period.

After steady state is reached in Fig. 11, the neutral stator current presents some distortion around zero. This is because the GSC is operating near its border of the voltage capability (i.e., overmodulation). Therefore, voltage saturation takes place, and perfect regulation is not possible. To avoid more significant effects, antiwindup was implemented in all the controllers.

Figs. 10 and 11 validate the dynamic behavior obtained in simulations shown in Figs. 7 and 8, respectively. In Fig. 12, the transient behavior of the double-resonant controllers is shown, validating the simulation result in Fig. 9. With a load imbalance, the full compensation is activated at 0.05 s. It is worth mentioning that the unbalanced currents of the stator are eliminated and that this imbalance is now in the GSC currents. Before the activation of the compensation, the unbalanced stator currents produce a small stator voltage (v_s) unbalance, as expected. Stator voltage is set to 270 V_{ll} by means of the stator d magnetizing flux control, i.e., 220 V_{peak} per phase, as well as it was done in simulations. This small voltage imbalance is reduced when the complete current imbalance is compensated for.

Elimination of negative-sequence currents in the DFIG reduces the undesirable effect of torque pulsations. An estimation of the torque pulsations is shown in Fig. 12, using expression (14). The torque pulsations occur when pulsating active power is demanded from the DFIG. An unbalanced load demands pulsating power, and any compensation strategy that achieves continuous active power delivered from the machine implies constant torque. Therefore, if loads still need a pulsation component of power, it must be supplied from the GSC. Consequently, pulsations in the dc-link voltage are anticipated. Fig. 12 shows this double-fundamental frequency pulsation in the dc link when torque pulsation is eliminated from the machine, i.e.,

$$\tau_e = \frac{3}{2}\frac{L_m}{N_M} p(i_{sd} i_{rq} - i_{rd} i_{sq}). \tag{14}$$

In Fig. 13, the behavior of the regulator of the dc-link voltage for the same experiment shown in Fig. 12 is shown. In Fig. 13(a), the reference current in the d-axis for the GSC (blue) present the actuation effect of the regulator in its low frequency (dc) component. The q component (green) has a mean value of zero (set point) and a pulsating component of 100 Hz that, along with the same frequency component in the d current, represent the negative-sequence compensation. The zero-sequence reference (red) is dominated by a component of 50 Hz from the imbalance and a component of 150 Hz of the third harmonic disturbance from the machine.

In Fig. 14, another class of load imbalance is tested. At near 0.05 s, an interruptor disconnects the load from phase a in order to take the i_{La} current to zero. Only phases b and c demand power from the system, and in steady state, the stator current is balanced due to the compensation control. A high-frequency ripple in phase a appears because no filter has been implemented at the stator side, and the two-level voltage disturbance from the GSC and DFIG becomes evident. In a practical implementation, a filter may be needed to reduce the effect of the commutation of the converters in

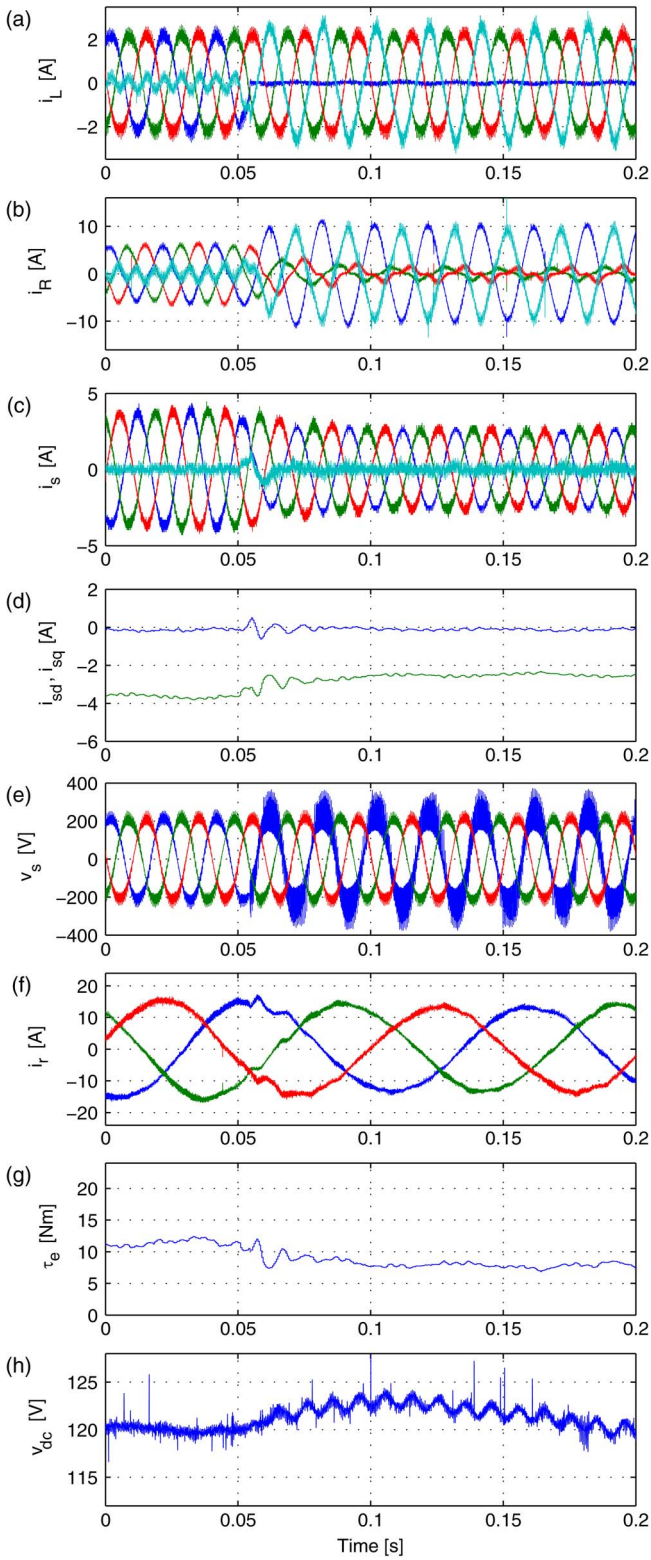

Fig. 14. Experimental load current imbalance disconnecting phase a. (a) Load currents. (b) GSC currents. (c) DFIG stator currents. (d) Positive flux SRF dq stator currents. (e) Stator voltages. (f) Rotor currents. (g) Torque. (h) DC-link voltage.

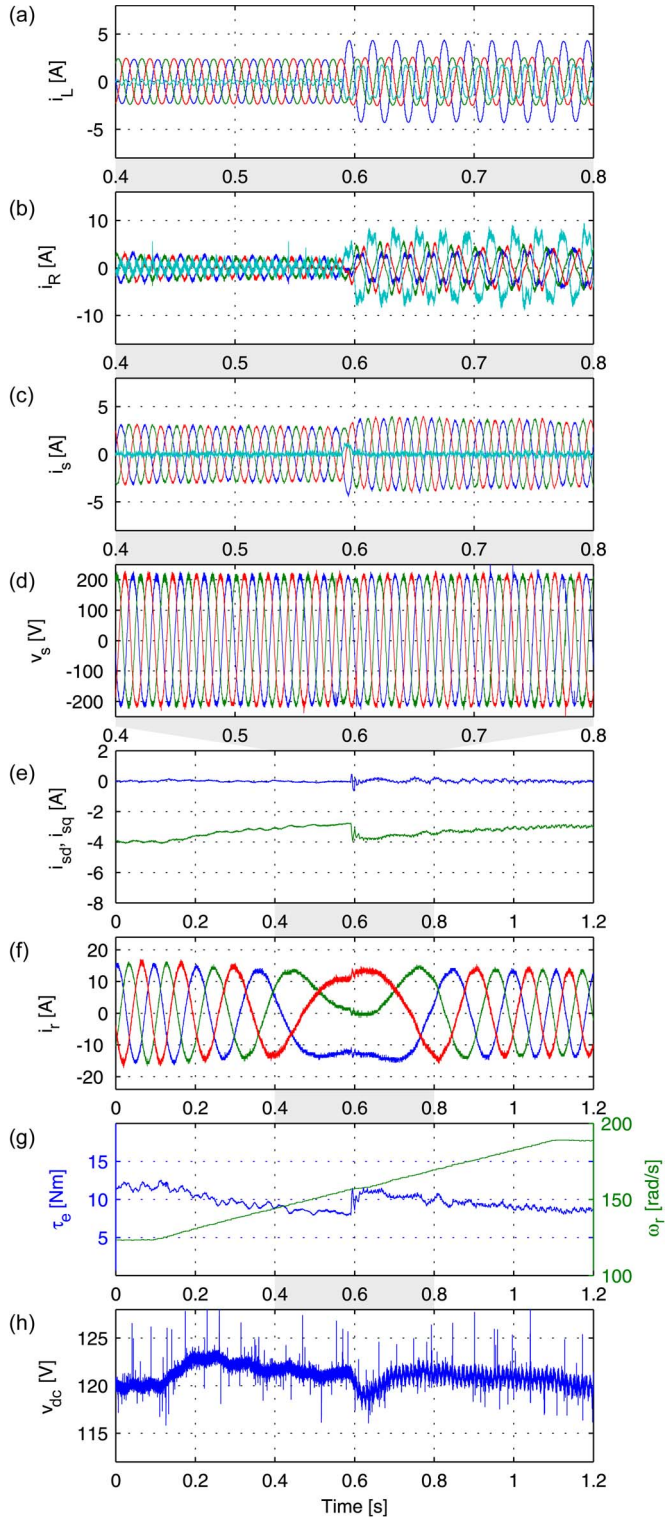

Fig. 15. Experimental load imbalance at variable speed. (a) Load currents. (b) GSC currents. (c) DFIG stator currents. (d) Positive SRF dq stator currents. (e) Stator voltages. (f) Rotor currents. (g) Torque and rotor angular speed. (h) DC-link voltage.

case of phase disconnection. In steady state, stator and rotor currents are sinusoidal, and torque has no ripple, although it decreases because lower power is demanded from the wind energy conversion system when one phase is disconnected. At subsynchronous speed, this reduction in power demanded from the doubly fed induction machine decreases the rotor power demanded from the RSC; thus, the dc-link voltage undergoes a transient disturbance as can be seen in Fig. 14(h) in addition to the expected double frequency ripple under load imbalance.

Finally, Fig. 15 shows a test under variable rotor speed. The compensation method is active at all times, and the load is unbalanced when the rotor speed is near 157 rad/s, i.e., synchronous speed. It is observed that the stator voltage remains nearly unaffected by the load change, and the stator currents are kept balanced after it. Rotor currents decrease when the rotor speed rises near synchronous speed even for a constant power load. At synchronous speed, no power exchange exists between the rotor and stator, and the rotor power consumption is only for power losses. The electric torque is reduced in order to keep the power constant as the speed increases; this continues until the load is changed. When the load is unbalanced, the GSC delivers the negative sequence to the load and is therefore highly unbalanced. The rotor currents have low distortion at all rotor speeds, and the dc link is kept near its set point of 120 V, reaching its exact set point when steady state is reached.

VI. Conclusion

In this paper, the need for current imbalance compensation in a DFIG for both reduction of torque pulsations and maximization of its current capability has been discussed. From the analysis and from simulation and experimental results, it is concluded that it is possible to reduce the torque pulsations in four-wire systems with only minor changes to the strategies previously proposed in the literature for three-wire systems. The mitigation of uneven heating of the stator windings in order to improve the total current capability of the generator is achieved by adding a neutral current compensation.

Based on the symmetrical components theory, a series of control strategies has been presented, ranging from SRF for positive-sequence current regulation and DSRF for positive- and negative-sequence current regulation to get to the use of resonant controllers in stationary abc coordinates. The equivalence of DSRF to resonant controllers in stationary frame, plus the simple addition of neutral current control, leads to the conclusion that the more appropriate strategy is the utilization of resonant controllers in abc coordinates. This leads to a natural decoupling of the phases in a four-wire connection. Moreover, the simplicity of implementation of resonant controllers in the abc frame allows a straightforward increase in the order of the controllers so as to compensate for additional current harmonic distortion using a multiresonant scheme. On the other hand, harmonic mitigation in a multiple SRF strategy would require significantly more complexity. This discussion shows that active filtering is the underlying general concept necessary to achieve compensation for imbalances in an isolated grid. Finally, from the empirical experience, it is concluded that an adequate tuning of resonances and a high sampling rate, i.e., a sufficiently high switching frequency, are both necessary in order to have good performance for active filtering. Otherwise, it becomes difficult to adjust a stable closed-loop control that includes all the desired resonances.

Appendix
Setup Parameters

See Tables I and II.

TABLE I
Circuit Parameters

GSC and RSC		DFIG	
R_F	0.4[Ω]	N_M	2.8
L_F	10[mH]	p	2
L_{F_f}	0[mH]	V_s	380 [V_{LL}]
R_L	94[Ω]	V_r	134 [V_{LL}]
L_L	0	P_N	4 [kW]
$C_{\text{dc-link}}$	5400[μF]	$\cos\phi$	0.8
v_{dc}	120[V]	i_{sN}	8.15 [A]
$\lvert\vec{v}_s\rvert$	220[V_{peak}]	L_m	266.6 [mH]
		$L_{\sigma s}$	8.31 [mH]
		$L_{\sigma r}$	8.31 [mH]
		R_s	0.617 [Ω]
		R_r	3.21 [Ω]

TABLE II
Filter Parameters

T_{s_i} (currents control)	0.5[ms]
T_{s_v} (v_{dc} control)	10[ms]
PI for rotor current control	BW_{cl}≈60[Hz]
KN0	1.724994873741583
KN1	-1.567834262066876
PI for magnetizing current	BW_{cl}≈1.4[Hz]
KN0	7.319648986340916
KN1	-7.298924877042699
PI for dc-link voltage control	BW_{cl}≈14[Hz]
KN0	0.292454265823508
KN1	-0.249551225027199
GSC current control	
KN0	8.686301502299527
KN1	-32.309945562987338
KN2	46.372247160710749
KN3	-30.444264691229403
KN4	7.700454365447873
KD1	-3.757389729567015
KD2	5.520147021340216
KD3	-3.757389729567029
KD4	1.000000000000000
HPF for GSC references filtering	$f_o = 25[Hz]$
KN0	0.962195245829104
KN1	-0.962195245829104
KD1	0.924390491658207
PLL PI controller	(BW_{cl}≈15Hz)
KN0	1.386059485264308
KN1	-1.365268592985344
PLL notch filter	$f_o = 100[Hz]$, $BW = 25[Hz]$
KN0	0.980399213259560
KN1	-1.864830120682292
KN2	0.980399213259560
KD1	1.864830120682292
KD2	-0.960798426519119

Acknowledgment

The authors would like to thank the Power Electronics, Machines, and Control Group of The University of Nottingham for providing the multiphase converter board used in this work.

References

[1] E. Muljadi, D. Yildirim, T. Batan, and C. Butterfield, "Understanding the unbalanced-voltage problem in wind turbine generation," in *Conf. Rec. 34th IEEE IAS Annu. Meeting*, 1999, vol. 2, pp. 1359–1365.

[2] L. Xu and Y. Wang, "Dynamic modeling and control of DFIG-based wind turbines under unbalanced network conditions," *IEEE Trans. Power Syst.*, vol. 22, no. 1, pp. 314–323, Feb. 2007.

[3] T. Brekken and N. Mohan, "A novel doubly-fed induction wind generator control scheme for reactive power control and torque pulsation compensation under unbalanced grid voltage conditions," in *Proc. IEEE PESC*, 2003, vol. 2, pp. 760–764.

[4] L. Xu, "Coordinated control of DFIG's rotor and grid side converters during network unbalance," *IEEE Trans. Power Electron.*, vol. 23, no. 3, pp. 1041–1049, May 2008.
[5] Y. Wang, L. Xu, and B. Williams, "Compensation of network voltage unbalance using doubly fed induction generator-based wind farms," *IET Renew. Power Gener.*, vol. 3, no. 1, pp. 12–22, Mar. 2009.
[6] Y. Liao, H. Li, J. Yao, and K. Zhuang, "Operation and control of a grid-connected DFIG-based wind turbine with series grid-side converter during network unbalance," *Elect. Power Syst. Res.*, vol. 81, no. 1, pp. 228–236, Jan. 2011.
[7] B. Singh and S. Sharma, "Design and implementation of four-leg voltage-source-converter-based VFC for autonomous wind energy conversion system," *IEEE Trans. Ind. Electron.*, vol. 59, no. 12, pp. 4694–4703, Dec. 2012.
[8] H.-S. Song and K. Nam, "Dual current control scheme for PWM converter under unbalanced input voltage conditions," *IEEE Trans. Ind. Electron.*, vol. 46, no. 5, pp. 953–959, Oct. 1999.
[9] A. Yazdani and R. Iravani, "A unified dynamic model and control for the voltage-sourced converter under unbalanced grid conditions," *IEEE Trans. Power Del.*, vol. 21, no. 3, pp. 1620–1629, Jul. 2006.
[10] V.-T. Phan, S.-H. Kwak, and H.-H. Lee, "An improved control method for DFIG-based wind system supplying unbalanced stand-alone loads," in *Proc. IEEE ISIE*, 2009, pp. 1081–1086.
[11] R. Pena, R. Cardenas, E. Escobar, J. Clare, and P. Wheeler, "Control strategy for a doubly-fed induction generator feeding an unbalanced grid or stand-alone load," *Elect. Power Syst. Res.*, vol. 79, no. 2, pp. 355–364, Feb. 2009.
[12] M. Pattnaik and D. Kastha, "Harmonic compensation with zero-sequence load voltage control in a speed-sensorless DFIG-based stand-alone VSCF generating system," *IEEE Trans. Ind. Electron.*, vol. 60, no. 12, pp. 5506–5514, Dec. 2013.
[13] R. Zhang, V. Prasad, D. Boroyevich, and F. Lee, "Three-dimensional space vector modulation for four-leg voltage-source converters," *IEEE Trans. Power Electron.*, vol. 17, no. 3, pp. 314–326, May 2002.
[14] M. Perales *et al.*, "Three-dimensional space vector modulation in abc coordinates for four-leg voltage source converters," *IEEE Power Electron. Lett.*, vol. 1, no. 4, pp. 104–109, Dec. 2003.
[15] J.-H. Kim and S.-K. Sul, "A carrier-based PWM method for three-phase four-leg voltage source converters," *IEEE Trans. Power Electron.*, vol. 19, no. 1, pp. 66–75, Jan. 2004.
[16] X. Li, Z. Deng, Z. Chen, and Q. Fei, "Analysis and simplification of three-dimensional space vector PWM for three-phase four-leg inverters," *IEEE Trans. Ind. Electron.*, vol. 58, no. 2, pp. 450–464, Feb. 2011.
[17] G. Saccomando and J. Svensson, "Transient operation of grid-connected voltage source converter under unbalanced voltage conditions," in *Conf. Rec. 36th IEEE IAS Annu. Meeting*, Chicago, IL, USA, 2001, vol. 4, pp. 2419–2424.
[18] V. Kaura and V. Blasko, "Operation of a phase locked loop system under distorted utility conditions," *IEEE Trans. Ind. Appl.*, vol. 33, no. 1, pp. 58–63, Jan./Feb. 1997.
[19] P. Rodriguez *et al.*, "Double synchronous reference frame PLL for power converters control," in *Proc. 36th IEEE PESC*, 2005, pp. 1415–1421.
[20] M. Karimi-Ghartemani and M. Iravani, "A method for synchronization of power electronic converters in polluted and variable-frequency environments," *IEEE Trans. Power Syst.*, vol. 19, no. 3, pp. 1263–1270, Aug. 2004.
[21] R. Pena, J. Clare, and G. Asher, "Doubly fed induction generator using back-to-back PWM converters and its application to variable-speed wind-energy generation," *Proc. Inst. Elect. Eng.—Elect. Power Appl.*, vol. 143, no. 3, pp. 231–241, May 1996.
[22] D. Zmood and D. Holmes, "Stationary frame current regulation of PWM inverters with zero steady-state error," *IEEE Trans. Power Electron.*, vol. 18, no. 3, pp. 814–822, May 2003.
[23] J. Hwang, P. Lehn, and M. Winkelnkemper, "A generalized class of stationary frame-current controllers for grid-connected ac–dc converters," *IEEE Trans. Power Del.*, vol. 25, no. 4, pp. 2742–2751, Oct. 2010.
[24] S. Muller, M. Deicke, and R. De Doncker, "Doubly fed induction generator systems for wind turbines," *IEEE Ind. Appl. Mag.*, vol. 8, no. 3, pp. 26–33, May/Jun. 2002.
[25] G. C. Goodwin, S. F. Graebe, and M. E. Salgado, *Control System Design*. Englewood Cliffs, NJ, USA: Prentice-Hall, 2000.

Gonzalo Carrasco was born in Santiago, Chile, in 1984. He received the B.Eng. degree in civil and electronic engineering from the Universidad Técnica Federico Santa María, Valparaíso, Chile, in 2008, where he is currently working toward the Ph.D. degree in electronic engineering.

César A. Silva (M'02) was born in Temuco, Chile, in 1972. He received the B.Eng. degree in electronic engineering from the Universidad Ténica Federico Santa María (UTFSM), Valparaíso, Chile, in 1998 and the Ph.D. degree from the Power Electronics Machines and Control Group, The University of Nottingham, Nottingham, U.K., in 2003.

Since 2003, he has been a Lecturer with the Departamento de Electrónica, UTFSM, where he teaches courses on electric machines theory, power electronics, and ac machine drives. His main research interests include sensorless vector control of ac machines and control of static converters.

Dr. Silva received the IEEE TRANSACTIONS ON INDUSTRIAL ELECTRONICS Best Paper Award in 2007.

Rubén Peña (S'95–M'97) was born in Coronel, Chile. He received the B.S.E.E. degree from the University of Concepción, Concepción, Chile, in 1984 and the M.Sc. and Ph.D. degrees from The University of Nottingham, Nottingham, U.K., in 1992 and 1996, respectively.

From 1985 to 2008, he was a Lecturer with the University of Magallanes, Punta Arenas, Chile. He is currently with the Electrical Engineering Department, University of Concepción. His main interests include control of power electronics converters, ac drives, and renewable energy systems.

Roberto Cárdenas (S'95–M'97–SM'07) was born in Punta Arenas, Chile. He received the B.S. degree from the University of Magallanes, Punta Arenas, in 1988 and the M.Sc. and Ph.D. degrees from The University of Nottingham, Nottingham, U.K., in 1992 and 1996, respectively.

During 1989–1991 and 1996–2008, he was a Lecturer with the University of Magallanes. From 1991 to 1996, he was with the Power Electronics Machines and Control Group, The University of Nottingham. During 2009–2011, he was with the Electrical Engineering Department, University of Santiago, Santiago, Chile. He is currently a Professor of power electronics and drives with the Electrical Engineering Department, University of Chile, Santiago. His main interests include control of electrical machines, variable-speed drives, and renewable energy systems.

Dr. Cárdenas received the Best Paper Award from the IEEE TRANSACTIONS ON INDUSTRIAL ELECTRONICS in 2005. He is an Associate Editor of the IEEE TRANSACTIONS ON INDUSTRIAL ELECTRONICS.